ROYAL SOCIETY OF CHEMISTRY

PAPER

Check for updates

Nano-alloying and nano-chemistry of the immiscible elements Fe and Cu in a FeSc–Cu nanoglass

Shiv Prakash Singh, [ID] *[ab] Mohammed Reda Chellali,[b] Torben Boll,[bcd] Herbert Gleiter[b] and Horst Hahn[b]

In this study, the alloying of immiscible elements, Fe and Cu, at the atomic level was studied using three-dimensional atom probe tomography (3D APT). The sample was prepared as nanoglass using the inert gas condensation technique with the thermal co-evaporation of $Fe_{90}Sc_{10}$ alloy and pure Cu. The final composition of the nanoglass was found to be $Fe_{75}Sc_{15}Cu_{10}$ by energy dispersive X-ray (EDX) spectroscopy. The X-ray diffraction (XRD) pattern indicated the amorphous nature of the sample. The APT analysis of the as-prepared sample showed a homogeneous mixture of Fe and Cu in the presence of Sc throughout the sample. The sample was heat-treated at 100, 200, and 400 °C to examine the miscibility limits with respect to temperature. The sample heat-treated at 100 °C showed a homogeneous distribution of the elements, but at higher temperatures at 200 and 400 °C it showed a de-alloying effect between Fe and Cu. It was observed that Sc tends to alloy with Fe up to 100 °C, but it tends to alloy with Cu at higher temperatures. This preferential alloying of Sc with Fe and Cu is explained by the heat of mixing of FeSc and CuSc alloys. This result will improve our understanding of the nano-alloying of immiscible elements.

1. Introduction

Understanding the formation of alloys and their atomic arrangement is of great interest for the materials science community. Most metallic alloys used in our daily life have a negative heat of mixing. In other words, the alloying of these elements is spontaneous at the atomic scale owing to the reduction of Gibbs free energy upon intermixing.[1,2] Alloys of immiscible elements provide an opportunity to synthesize a new class of materials with interesting properties and potential applications, such as in structural, catalytic, magnetic, thermal, and electrical applications.[2,3] To date, only a few techniques have been reported on the alloying of immiscible elements. Most studies were limited to the X-ray diffraction technique to characterize these materials.[4] Transmission electron microscopy (TEM) was also helpful in visualizing atomic arrangements in two dimensions.[5] Ma *et al.*[6] have reported the mechanical alloying of immiscible elements, such as Ag–Fe and Cu–Fe. In this study, Cu–Fe underwent atomic-level alloying, leading to the formation of solid solutions, whereas Ag–Fe remained largely unreacted. Another computational study reported that the weak interaction between Fe and Cu is comparable to a dangling bond.[7] The weak interaction resulted in the precipitation of Cu due to the Fe spin-polarization. The polarization results in a decrease in charge density and exhibits a weaker bond between Fe and Cu. It was described that the presence of Ni at the interfaces between Fe and Cu stabilizes the system enthalpy.

In crystalline phase, the formation of alloys with elements having a positive heat of mixing is quite difficult. They have stable ordered atomic structures, are at thermodynamical equilibrium, and possess the lowest energy state.[2,8] It is known that amorphous (or glassy) materials are disordered, non-equilibrium, and meta-stable materials.[9–13] Therefore, alloying could be easier for amorphous materials compared to thermodynamically stable crystalline materials. Some reports of the mixing of immiscible elements in the amorphous state are available.[14–18] He *et al.*[19] have reported the amorphous structures in the Ag–Ni system with a strong liquid immiscibility. They prepared the samples in the form of foils of about 10 μm thickness by DC sputtering on a liquid nitrogen-cooled silicon wafer. Subsequently, the vapor that was quenched in the phase-separated Ag–Ni system created alloys that appeared

[a] *Center for Advanced Ceramic Materials, International Advanced Research Center for Powder Metallurgy and New Materials, Balapur PO, Hyderabad, 500005, India. E-mail: spsingh67@gmail.com*

[b] *Institute of Nanotechnology, Karlsruhe Institute of Technology, Hermann-von-Helmholtz-Platz 1, 76344, Eggenstein-Leopoldshafen, Germany*

[c] *Institute for Applied Materials (IAM-WK), Karlsruhe Institute of Technology (KIT), Engelbert-Arnold-Str. 4, 76131, Karlsruhe, Germany*

[d] *Karlsruhe Nano Micro Facility (KNMFi), Karlsruhe Institute of Technology (KIT), Hermann-von-Helmholtz-Platz 1, 76344, Eggenstein-Leopoldshafen, Germany*

homogeneous and amorphous under the conventional probe techniques. However, structural analysis at the atomic level using extended X-ray absorption fine structures combined with the reverse Monte Carlo and molecular dynamics simulations revealed that the phases were heterogeneous and have spinodal-like structures on an extremely fine scale. Wang et al.[20] have reported the formation of an amorphous phase in an immiscible system of Cu–Nb by the ion mixing technique and molecular dynamics (MD) simulations. An n-body potential was constructed and applied to investigate the crystal-to-amorphous transition in the immiscible system of Cu–Nb by MD simulations. It was demonstrated that in the composition range of 15–72 at%, Nb goes into a disordered state forming an amorphous alloy. Moreover, it was found that $Cu_{70}Nb_{30}$ and $Cu_{30}Nb_{70}$ amorphous alloys were formed upon ion beam mixing using multilayer films.

A new kind of amorphous material known as nanoglass has been reported. The nanoglass comprises two structures: a glassy core and a glass–glass interface.[21–23] Nanoglass exhibits a stable structure and exciting properties compared to the conventional glass of the same chemical composition. Chen et al.[24] have reported the alloying of immiscible elements, Fe and Cu, by mixing FeSc and CuSc nanoglass alloys using the inert gas condensation (IGC) technique. The magnetic properties were tuned by adjusting the composition of the FeSc alloy. The change in the magnetic properties was explained with the help of a reduction in the volume fraction of the glass–glass interfaces of FeSc nanoglass with an increase in the CuSc nanoglass. Hence, understanding the structure of such materials of immiscible elements at the atomic level is interesting.

In view of the above, we studied the alloying of Fe and Cu at the atomic level in the presence of Sc using APT. The spatial resolution of APT permits the investigation of the alloying of Fe and Cu. The diffusion of Cu in the nanoglass at different annealing temperatures has also been explored. This study will provide information on the microstructure evolution upon annealing for the nanoglass alloy of Fe and Cu.

2. Synthesis and characterization

The nanoglass alloy of the immiscible elements (Fe and Cu) was prepared using two tungsten crucibles in an inert gas condensation (IGC) chamber. The crucibles were placed parallel to each other to obtain co-evaporation from both. An ingot of 2 g weight of $Fe_{90}Sc_{10}$ (at%) alloy was prepared using high purity chemicals (99.9%, ChemPure) by repetitive arc melting under an Ar atmosphere and placed on the boat. Another boat was filled with 1 g of pure copper metal (99.9%, ChemPure). The base pressure of the IGC chamber was maintained at 3×10^{-8} mbar to ensure the purity of the product. Before the co-evaporation of $Fe_{90}Sc_{10}$ and Cu from the two crucibles, the parameters such as power, time, and the rate of evaporation of each alloy/element were standardized by performing individual evaporation experiments. Subsequently, both crucibles were heated electrically to co-evaporate the $Fe_{90}Sc_{10}$ alloy and copper by controlling the power supply to the individual crucible to

mix them in the gas phase. The chamber pressure of 5 mbar was maintained during the evaporation by introducing high purity (99.9999%) He gas. In the periodic table, He is the second lightest element after hydrogen. During the synthesis of nanoglass in IGC chamber, evaporated FeSc and Cu collided with the He atoms inside the IGC chamber, lost their kinetic energy, and formed small particles down to 10–15 nm.[25] Due to the nm sized small particles, a faster quenching process promotes the formation of glassy nanoparticles. The amorphous nanoparticles ($\sim$10–15 nm) were deposited on a liquid nitrogen-cooled cylinder (cold-finger) by the convective flow of the He gas. Subsequently, the amorphous powder was scraped from the cold finger and collected in a holder. The collected powder was compacted in situ at a uniaxial pressure of 3 GPa in an 8 mm die at 2×10^{-8} mbar pressure.

The diffusion of elements in the above prepared nanoglass sample at different temperatures was studied by heat-treating it at 100, 200, and 400 °C for 3 h in a tubular furnace under 3×10^{-9} mbar pressure. The final chemical composition of the prepared nanoglass specimen was investigated by EDX spectroscopy equipped with the field emission scanning electron microscopy (FESEM) instrument (LEO 1530). X-ray diffraction (XRD) was accomplished using a Philips (X'Pert) diffractometer (Mo Kα X-ray source) operated at 45 kV and 40 mA. The atomic arrangement and chemical composition of the sample were analyzed by APT. The lamella tip for APT characterization was prepared by a standard lift-out method in a Zeiss Auriga 60 focused ion beam (FIB) instrument. The annular milling produced the needle-shaped APT sample with a typical curvature radius of about 100 nm and a height of about 350 nm. Finally, to ensure a low Ga content in the APT sample, the final FIB "clean-up" procedure was carried out at low voltage (5 kV). The APT measurements were performed using a Cameca-LEAP 4000X HR instrument in the laser pulsing mode with the following operational parameters: laser wavelength 355 nm, pulse frequency 100 kHz, sample temperature 60 K, pulse energy 50 pJ, and evaporation rate 0.5%. The collected APT experimental data were reconstructed using the software package IVAS 3.6.14. Isoconcentration surface and proxigram concentration profile analysis were applied to determine the explicit areas and depict concentration profiles, respectively, using APT data. Isoconcentration surface analysis was done on the surfaces drawn in the 3-D reconstruction with a particular range of signal intensities of an indicated ion at an isolated areas.[26–28] A proxigram (i.e., proximity histogram) is related to a 1-D concentration profile, but it estimates a concentration profile pertaining to distance from a particular isoconcentration surface.[28–30]

3. Results and discussion

$Fe_{90}Sc_{10}$ alloy was chosen in this study owing to its good glass-forming composition.[31,32] Elemental Cu was evaporated and mixed with $Fe_{90}Sc_{10}$ in IGC chamber to form an amorphous alloy. The role of Sc was to promote the glass formation and hinder the crystallinity in the prepared sample. As mentioned

above, the final composition of the prepared nanoglass was investigated by EDX spectroscopy coupled with FESEM instrument. The composition of $Fe_{75}Sc_{15}Cu_{10}$ was found by the elemental scanning of the FESEM image of an area of 2000 × 2000 μm². Moreover, XRD analysis was carried out to explore the nature of the sample. Fig. 1 shows the XRD pattern of the as-prepared nanoglass with the composition of $Fe_{75}Sc_{15}Cu_{10}$. The XRD analysis does not offer any distinct sharp peak of a crystalline structure. Although the XRD pattern corresponds to an amorphous phase, a small crystalline phase cannot be denied according to the previous study by Chen et al.[24] Chen et al. reported evidence of the amorphous nature from TEM study. Thus, we believe that the prepared sample was primarily amorphous. This study further explored the nano-chemistry and atomic arrangements of Fe and Cu in three-dimensional space. Hence, our study focused on the atomic structure of Fe and Cu using three-dimensional techniques at the nano-scale in the presence of Sc.

To explore the atomic-scale structure and chemistry of the $Fe_{75}Se_{15}Cu_{10}$ nanoglass, three-dimensional (3D) APT was employed. The APT analysis for the as-prepared nanoglass is displayed in Fig. 2. The atomic reconstruction depicted a homogeneous distribution of all three elements (Fe, Sc, and Cu) throughout the sample within the nano-scale limits (Fig. 2(a)). The concentration fluctuations for the constituent elements are presented in Fig. 2(b). A concentration variation of Fe, Sc, and Cu compositions were found to be 74–78, 12–15, and 8–10 at%, respectively. The most important observation from this result was that the two immiscible elements Fe and Cu alloyed at ambient temperature despite their positive heat of mixing.

To understand the alloying of Fe and Cu under different thermal conditions, we have extended the study to explore the behavior of Fe and Cu at different temperatures. Hence, the nanoglass sample $Fe_{75}Sc_{15}Cu_{10}$ was heat-treated at 100, 200, and 400 °C for 3 hours each. The APT experimental results of the heat-treated specimens are discussed as follows:
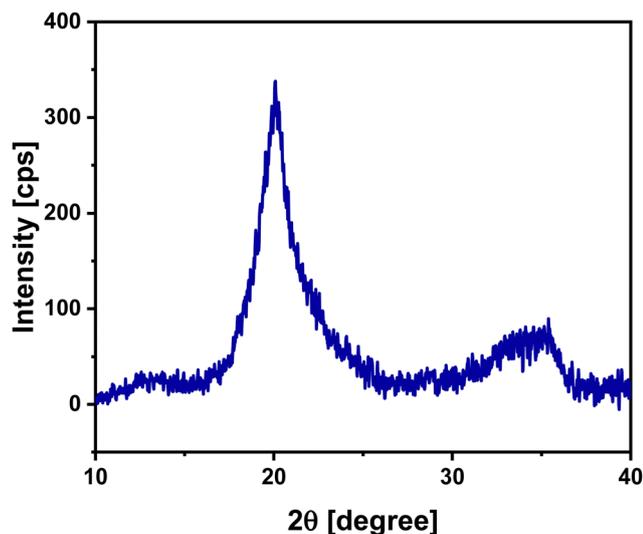

Fig. 1 X-ray diffraction pattern of the as-prepared nanoglass of $Fe_{75}Sc_{15}Cu_{10}$.

Fig. 3 shows the APT elemental analysis for the sample heat-treated at 100 °C per 3 h. Fig. 3(a) demonstrates the homogeneous elemental distribution of Fe, Sc, and Cu. Furthermore, the elemental distribution of Fe and Cu and Sc are displayed in Fig. 3(b) and (c), respectively. These results show that Fe and Cu are forming a solid solution. The proxigram concentration profile in Fig. 3(d) for an isosurface of 38 at% Cu shows that Cu concentration reaches 80 at%, and there is a decrease in the content of Fe to 20 at%. This reveals a large concentration gradient for Fe and Cu. The Sc concentration follows the decreasing trend of Fe. This shows that Sc alloys with Fe as it was the initial composition ($Fe_{90}Sc_{10}$) in the ingot. The result of the proxigram compared with the as-prepared nanoglass shows that Cu has agglomerated by diffusion at 100 °C. However, Sc maintains an average concentration of 15 at%. Hence, the concentration gradient has decreased for Fe and Cu compared to the as-prepared nanoglass.

The as-prepared nanoglass was further heat-treated at 200 °C for 3 hours, and its APT images are depicted in Fig. 4. The heat-treated nanoglass shows the concentration gradient between Fe and Cu visualized in Fig. 4(a). The 2D elemental map image shows that the concentration of Fe and Sc is homogenous in most sample regions with marginal fluctuations. However, Cu shows agglomeration, which suggests comparatively faster diffusion of Cu. The concentration profile in Fig. 4(c) also significantly fluctuates between the high Fe and Cu regions. The concentration of Fe and Cu vary in the range of 80–40 and 10–40 at%, respectively, which indicates the de-alloying of Fe and Cu. The slope of Sc concentration inclines to the Cu concentration profile. This differs from the 100 °C heat-treated sample, where the Sc concentration profile followed the Fe profile. This suggests that Sc prefers to alloy with Cu at elevated temperatures. The proxigram concentration profile in Fig. 4(d) for an isosurface of 25 at% Cu and 20 at% Sc displays the concentration of Cu extended up to 60 at% and Fe to 20 at%.

The above findings motivated further heat treatment to perceive the thermal effect on the configuration of Fe and Cu. Hence, the prepared nanoglass $Fe_{75}Sc_{15}Cu_{10}$ was heat-treated at 400 °C for 3 hours. The APT results for the nanoglass sample heat-treated at 400 °C are displayed in Fig. 5. The elemental mapping for Fe, Sc, and Cu shows the segregation of Cu in Fig. 5(b and c). The concentration profile in Fig. 5(d) shows a large fluctuation of Fe and Cu in the range of 90–10 at% and 7–60 at%, respectively, throughout the sample. This fluctuation indicates the independent segregation of Fe and Cu in the sample. The concentration profile of Sc showed a similar trend as that of Cu, which indicated that Sc was alloying with Cu. The proxigram images in Fig. 5(e) confirm the chemical composition of the particle to be 80 at% Cu with 0 at% Fe. Hence, after the 400 °C heat treatment, Fe and Cu are entirely de-alloyed.

The two immiscible elements, Fe and Cu, were alloying at the nano-scale in the amorphous phase at room temperature, which was difficult in the crystalline form (equilibrium state). The Miedema model predicts that the heat of mixing for $Fe_{50}Cu_{50}$ alloy is +22 kJ mol⁻¹. The enhanced alloying of Fe–Cu needed sufficient driving force (energy) to overcome this
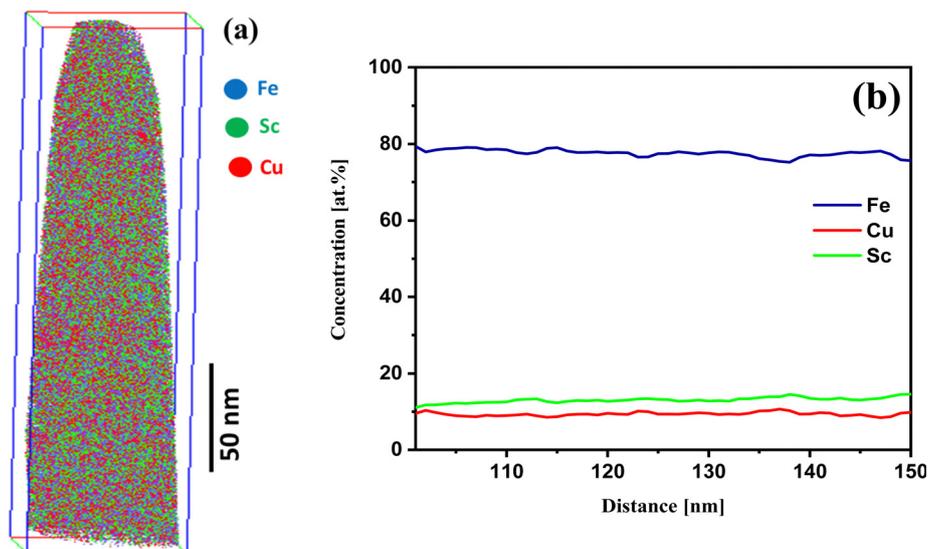
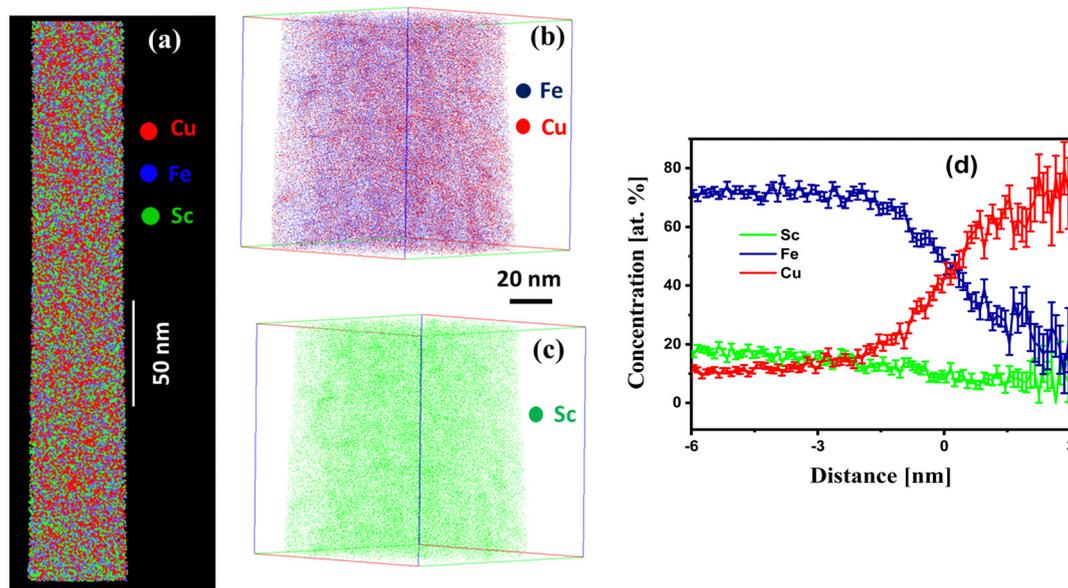Fig. 2   (a) APT image and (b) the concentration profile of the as-prepared nanoglass of $Fe_{75}Sc_{15}Cu_{10}$.

Fig. 3   (a) APT image, the elemental distribution map of (b) Fe and Cu and (c) Sc of prepared $Fe_{75}Sc_{15}Cu_{10}$ nanoglass heat-treated at 100 °C for 3 hr. (d) Proxigram concentration profile for the isosurface of 38 at% Cu.

large positive heat of mixing. Some studies on the alloying of the Fe–Cu alloy in the metastable state have been reported. Chen *et al.*[24] have reported the alloying of the Fe and Cu at the nano-scale in the $Fe_{90}Sc_{10}$–$Cu_{64}Sc_{36}$ nanoglass prepared by the inert gas condensation method. They intermixed the two nanoglasses of $Fe_{90}Sc_{10}$ and $Cu_{64}Sc_{36}$ and tuned the properties. Moreover, the evidence for the amorphous state and their solid-state mixing are provided by TEM images and elemental mapping. The magnetic property was controlled by adjusting the interfaces between the $Fe_{90}Sc_{10}$ nanoglass particles. It has been discussed that a positive heat of mixing between Fe and Cu limits spontaneous mixing in wide composition ranges.

Therefore, an additional driving force for mixing these immiscible elements is required. Moreover, they reported a change in the magnetic properties by varying the interfacial density of the $Fe_{90}Sc_{10}$–$Cu_{64}Sc_{36}$ nanoglass alloy, specifically an increase in the magnetization from 0.63 µB per Fe atom to 1.12 µB per Fe atom at an external field of 20 kOe, when the $Fe_{90}Sc_{10}$ constituent rises from 23 to 74 at%. Any further introduction of the $Cu_{64}Sc_{36}$ nanoglass reduces the possibility for the mutual contact of $Fe_{90}Sc_{10}$ nanoparticles, thus reducing the interfaces between the $Fe_{90}Sc_{10}$ nanoparticles. This fact confirms the effect of the interfaces on ferromagnetism, which succeeds over the contribution of the nanoglass cores. It is found that the magnetization
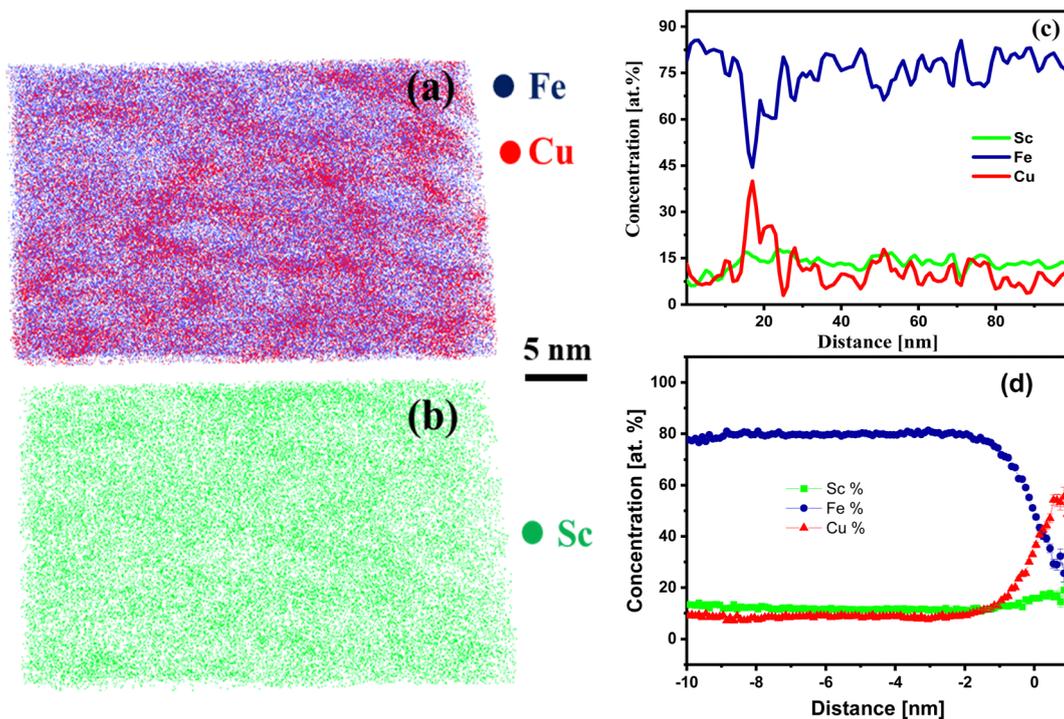
Fig. 4 APT image (a) elemental mapping of both Fe and Cu as well as for (b) Sc, and (c) the concentration profile of the heat-treated sample as-prepared nanoglass of $Fe_{75}Sc_{15}Cu_{10}$ at 200 °C for 3 h; (d) Proxigram concentration profile for the isosurface of 25 at% Cu and 20 at% Sc.

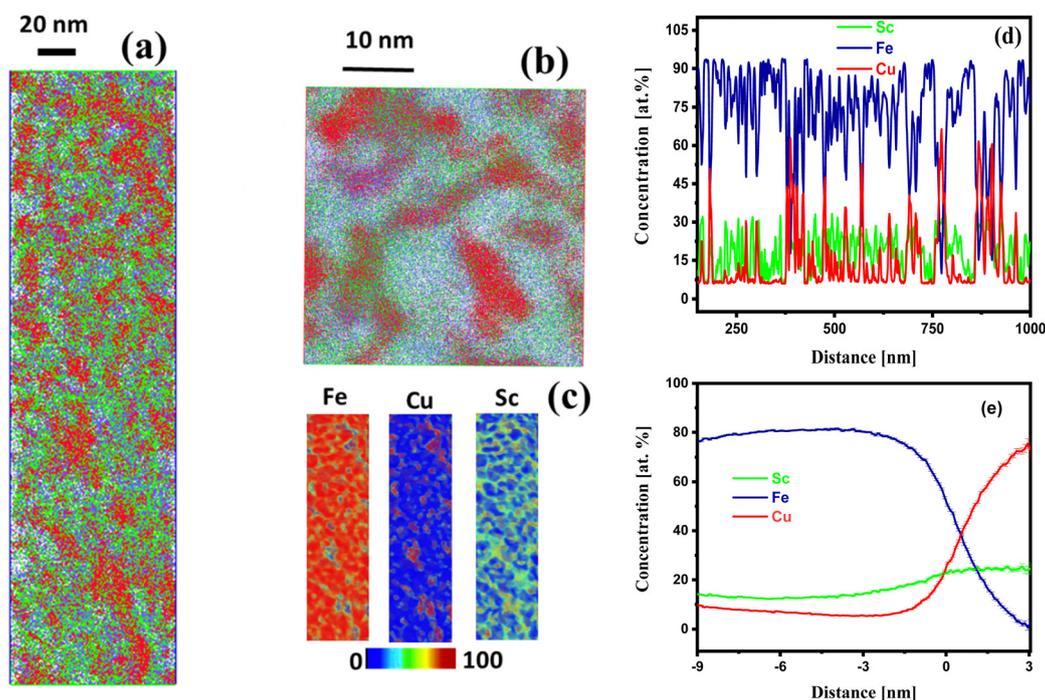**Fig. 5** (a and b) APT images of $Fe_{75}Sc_{15}Cu_{10}$ nanoglass heat-treated at 400 °C for 3 hr; (c) elemental heat maps for Fe, Cu, and Sc; (d) the concentration profiles of the heat-treated sample, and (e) proxigram concentration profile for the three elements as mentioned above.

of the $(Fe_{90}Sc_{10})_{0.74}(Cu_{64}Sc_{36})_{0.26}$ nanoglass alloy is superior to the pure $Fe_{90}Sc_{10}$ nanoglass *i.e.*, 1.05 μB per Fe atom. With the initial addition of the $Fe_{90}Sc_{10}$ component in the above two-component nanoglass, the magnetism increases. However, a decreasing trend dominates for the compositions above 75 at%. In our study, Fe was found as bcc and Cu as fcc phases

at room temperature. However, the XRD pattern in Fig. 1 does not show distinct peaks for Fe and Cu. This indicated the formation of a supersaturated solid solution of Fe, Cu, and Sc in the amorphous phase. Kozeschnik[33] revealed that the interfacial energy of the nanometer-sized Cu of unlike compositions of Fe–Cu alloy plays a vital role in the precipitation of Cu. It emphasized that the nanometer precipitation differs from the large precipitations of Cu.

In this study of $Fe_{75}Sc_{15}Cu_{10}$ nanoglass, the size of the glassy clusters forming the nanoglass was in the nanometer range (10–15 nm). Hence, it created a large interfacial density in the nanometer scale and formed a high-energy metastable state. Moreover, the nanoglass has a high free volume in these interface regions.[21] The high interfacial energy and large interfacial free volume seem to be the driving force for the intermixing of the Fe and Cu in the presence of Sc. However, this alloying is limited to the 10 at% of Cu in the $Fe_{75}Sc_{15}Cu_{10}$ nanoglass using the IGC technique. This homogeneous mixing of Fe and Cu at the nano-scale is demonstrated by the 3D APT study as presented in Fig. 2. Other methods, such as mechanical alloying, also reported the alloying of Cu and Fe in the solid state. Quelennec et al.[34] have demonstrated the alloying of Fe and Cu by high-pressure torsion and found a homogeneous supersaturated solid solution of 12% Fe in the fcc Cu. Copper ferroalloys (CFA) were prepared by Zhang et al.[35] using the powders of Fe and Cu through mechanical alloying and vacuum sintering, followed by the hot and cold rolling process. It is demonstrated that up to 10 wt% Fe dissolved in fcc Cu after annealing. Moreover, Fe precipitated in the 30 wt% Fe containing CFA and it was found that mechanical alloying was analogous with the other reports.[36,37] Puthucode et al.[38] have studied the de-vitrification of the phase separated immiscible Cu–Nb amorphous thin film at the nanoscale using TEM and APT experimental results. The TEM and APT results revealed that the amorphous Cu–Nb undergoes a two stage crystallization process at 200 and 300 °C resulting in crystalline Cu rich fcc and the spherulitic grain of bcc phases, respectively, for Cu–45 at% Nb composition in the amorphous matrix. The compositional partition between the phases formed at different annealing temperatures has been plotted by a normalized frequency distribution plot using the APT data. In another study, Banerjee et al.[39] demonstrated the direct evidence of the nanoscale phase separation of immiscible Cu–Nb amorphous thin film using APT studies. The results obtained by APT demonstrated that the nanoscale phase separation is responsible for the stabilization of the amorphous phases.

In the present study, upon increasing the heat-treatment temperatures to 100, 200, and 400 °C, the two elements Fe and Cu de-alloy gradually. Heating at 100 °C, Fe and Cu were still homogeneously distributed at the nano-scale throughout the sample. However, with an increase in the temperatures to 200 °C, the Fe–Cu alloy started to de-alloy and this was more prominent at 400 °C (Fig. 4 and 5). The thermal diffusion of Cu directed the de-alloying mechanism. In the nanoglass, the free volume was available at the interfaces that facilitate the fast diffusion of Cu through the interfacial path. At 400 °C, Fe and Cu were precipitated separately and showed the immiscibility gap in the crystalline form. With the increase in the heat-treatment temperature, it was interesting that the third element Sc was more prone to alloy with Fe at room temperature, however, it tended to form an alloy with Cu at elevated temperatures. The heat of mixing for Fe–Sc and Cu–Sc alloy confirmed this fact. The Miedema model calculated the heat of mixing for Fe–Sc and Cu–Sc as −17 and −43 kJ mol^{-1}, respectively.[1] It manifested that Cu–Sc has a higher negative heat of mixing than Fe–Sc. Hence, it favors the formation of the Cu–Sc alloy at elevated temperatures. The schematic presentation of the above process is presented in Fig. 6. The system changed from a non-equilibrium state (amorphous) to a stable equilibrium state (crystalline) with increasing thermal treatment. Although it is not within the scope of the current study, it will be interesting to see the effect of temperature on the change in the Fe and Cu phases (e.g., bcc and fcc) at elevated temperature by XRD or TEM analysis in future work.

4. Conclusions

This study demonstrates the mixing of immiscible elements at the atomic level using 3D APT. The sample was prepared using the inert gas condensation technique of thermal co-evaporation with two parallel-arranged crucibles. The two boats were filled
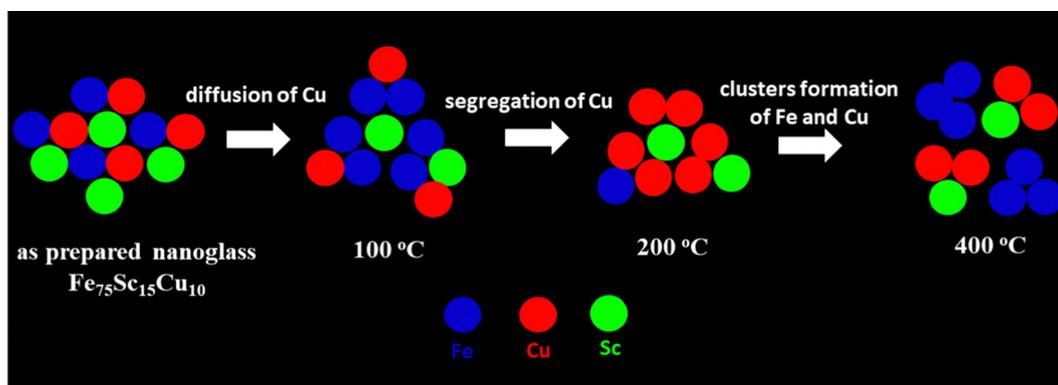

Fig. 6 Schematic illustration of the thermal effect (at 100, 200, and 400 °C) on the atomic structure of the $Fe_{75}Sc_{15}Cu_{10}$ nanoglass.

with $Fe_{90}Sc_{10}$ alloy and pure Cu ingots and subsequently co-evaporated for mixing in the gaseous state. The prepared sample has the $Fe_{75}Sc_{15}Cu_{10}$ composition and characteristic nanoglass structure. X-ray diffraction result showed the amorphous nature of the prepared nanoglass. The prepared nanoglass was heat-treated at 100, 200, and 400 °C for 3 hr. APT results of the as-prepared nanoglass show the homogeneous distribution of Fe, Sc, and Cu throughout the sample and a Cu alloy with Fe up to 10 at%. The concentration fluctuations of Fe and Cu increased with the thermal treatment temperature. The sample heat-treated at 400 °C showed the complete de-alloying of Fe and Cu. In the concentration profile at lower annealing temperatures (*i.e.* at 100 °C), Sc followed the concentration profile of Fe, but at elevated temperature (*i.e.*, at 400 °C) it followed that of Cu. This observation suggests that the Sc remained with Cu at the interfaces, while the core is iron-rich at 400 °C. This has been explained in terms of the heat of mixing of FeSc and CuSc.

Conflicts of interest

There are no conflicts to declare.

Acknowledgements

References

1 A. R. Miedema, Heat of Formation of Alloys, *Philips Tech. Rev.*, 1976, **36**(8), 217–231.

2 E. Ma, Alloys Created between Immiscible Elements, *Prog. Mater. Sci.*, 2005, **50**(4), 413–509.

3 A. Caro, M. Caro, E. M. Lopasso, P. E. A. Turchi and D. Farkas, Thermodynamics of Fe-Cu Alloys as Described by a Classic Potential, *J. Nucl. Mater.*, 2006, **349**(3), 317–326.

4 A. A. Bunaciu, E. G. UdriŞTioiu and H. Y. Aboul-Enein, X-Ray Diffraction: Instrumentation and Applications, *Crit. Rev. Anal. Chem.*, 2015, **45**(4), 289–299.

5 H. L. Fraser, D. W. McComb and R. E. A. Williams, Transmission Electron Microscopy for Physical Metallurgists, *Physical Metallurgy*, Elsevier, 2014, pp. 1143–1226.

6 E. Ma, J. He and P. J. Schilling, Mechanical Alloying of Immiscible Elements: Ag-Fe Contrasted with Cu-Fe, *Phys. Rev. B: Solid State*, 1997, **55**(9), 5542–5545.

7 W. Song and S. Zhao, Spin Polarization Gives Rise to Cu Precipitation in Fe-Matrix, *Phys. Chem. Chem. Phys.*, 2014, **16**, 7222–7230.

8 J. M. Monti, E. M. Hopkins, K. Hattar, F. Abdeljawad, B. L. Boyce and R. Dingreville, Stability of Immiscible Nanocrystalline Alloys in Compositional and Thermal Fields, *Acta Mater.*, 2022, **226**, 117620.

9 E. Ma, Tuning Order in Disorder, *Nat. Mater.*, 2015, 547–552.

10 M. Simoncelli, N. Marzari and F. Mauri, Unified Theory of Thermal Transport in Crystals and Glasses, *Nat. Phys.*, 2019, **15**(8), 809–813.

11 G. Biroli, J. P. Bouchaud, A. Cavagna, T. S. Grigera and P. Verrocchio, Thermodynamic Signature of Growing Amorphous Order in Glass-Forming Liquids, *Nat. Phys.*, 2008, **4**(10), 771–775.

12 P. G. Debenedetti and F. H. Stillinger, Supercooled Liquids and the Glass Transition, *Nature*, 2001, **410**, 259–267.

13 D. B. Miracle, A Structural Model for Metallic Glasses, *Nat. Mater.*, 2004, **3**(10), 697–702.

14 R. Najafabadi, D. J. Srolovitz, E. Ma and M. Atzmon, Thermodynamic Properties of Metastable Ag-Cu Alloys, *J. Appl. Phys.*, 1993, **74**(5), 3144–3149.

15 V. Elofsson, G. A. Almyras, B. Lü, R. D. Boyd and K. Sarakinos, Atomic Arrangement in Immiscible Ag–Cu Alloys Synthesized Far-from-Equilibrium, *Acta Mater.*, 2016, **110**, 114–121.

16 V. Petkov, B. N. Wanjala, R. Loukrakpam, J. Luo, L. Yang, C. J. Zhong and S. Shastri, Pt-Au Alloying at the Nanoscale, *Nano Lett.*, 2012, **12**(8), 4289–4299.

17 L. C. Wei and R. S. Averback, Phase Evolution during Ion-Beam Mixing of Ag-Cu, *J. Appl. Phys.*, 1997, **81**(2), 613–623.

18 W. Zhang, S. Zhuang, L. Liao, H. Dong, N. Xia, J. Li, H. Deng and Z. Wu, Two-Way Alloying and Dealloying of Cadmium in Metalloid Gold Clusters, *Inorg. Chem.*, 2019, **58**(9), 5388–5392.

19 J. H. He, H. W. Sheng, P. J. Schilling, C. Chien and E. Ma, Amorphous Structures in the Immiscible Ag-Ni System, *Phys. Rev. Lett.*, 2001, **86**(13), 2826–2829.

20 T. L. Wang, J. H. Li, K. P. Tai and B. X. Liu, Formation of Amorphous Phases in an Immiscible Cu – Nb System Studied by Molecular Dynamics Simulation and Ion Beam Mixing, *Scr. Mater.*, 2007, **57**, 157–160.

21 H. Gleiter, Nanoglasses: A New Kind of Noncrystalline Material and the Way to an Age of New Technologies?, *Small*, 2016, **12**(16), 2225–2233.

22 H. Gleiter, Nanoglasses: A New Kind of Noncrystalline Materials, *Beilstein J. Nanotechnol.*, 2013, **4**(1), 517–533.

23 N. Chen, D. V. Louzguine-Luzgin and K. Yao, A New Class of Non-Crystalline Materials: Nanogranular Metallic Glasses, *J. Alloys Compd.*, 2017, **707**, 371–378.

24 N. Chen, D. Wang, T. Feng, R. Kruk, K.-F. Yao, D. V. Louzguine-Luzgin, H. Hahn and H. Gleiter, A Nanoglass Alloying Immiscible Fe and Cu at the Nanoscale, *Nanoscale*, 2015, **7**(15), 6607–6611.

25 C. Suryanarayana and B. Prabhu, in Synthesis of Nanostructured Materials by Inert-Gas Condensation Methods, *Nanostructured Materials: Processing, Properties, and Applications*, ed. C. C. Koch, William Andrew Inc., 2007, pp. 47–90.

26 B. Gault, M. P. Moody, J. M. Cairney and S. P. Ringer, *Atom Probe Microscopy, Springer Series in Materials Science*, Springer New York, New York, NY, 2012, vol. 160.

27 D. N. Seidman, Three-Dimensional Atom-Probe Tomography: Advances and Applications, *Annu. Rev. Mater. Res.*, 2007, **37**, 127–158.

28 B. Gault, M. P. Moody, J. M. Cairney and S. P. Ringer, in Analysis Techniques for Atom Probe Tomography, *Atom Probe Microscopy*, Springer Science + Business Media, New York, 2012, vol. 160, pp. 213–297.

29 O. C. Hellman, J. A. Vandenbroucke, J. Rüsing, D. Isheim and D. N. Seidman, Analysis of Three-Dimensional Atom-Probe Data by the Proximity Histogram, *Microsc. Microanal.*, 2000, **6**(5), 437–444.

30 S. S. Rout, P. R. Heck, D. Isheim, T. Stephan, N. J. Zaluzec, D. J. Miller, A. M. Davis and D. N. Seidman, Atom-Probe Tomography and Transmission Electron Microscopy of the Kamacite–Taenite Interface in the Fast-Cooled Bristol IVA Iron Meteorite, *Meteorit. Planet. Sci.*, 2017, **52**(12), 2707–2729.

31 R. Witte, T. Feng, J. X. Fang, A. Fischer, M. Ghafari, R. Kruk, R. A. Brand, D. Wang, H. Hahn and H. Gleiter, Evidence for Enhanced Ferromagnetism in an Iron-Based Nanoglass, *Appl. Phys. Lett.*, 2013, **103**(7), 073106.

32 M. Ghafari, S. Kohara, H. Hahn, H. Gleiter, T. Feng, R. Witte and S. Kamali, Structural Investigations of Interfaces in Fe 90Sc 10 Nanoglasses Using High-Energy x-Ray Diffraction, *Appl. Phys. Lett.*, 2012, **100**(13), 2–6.

33 E. Kozeschnik, Thermodynamic Prediction of the Equilibrium Chemical Composition of Critical Nuclei: Bcc Cu Precipitation in α-Fe, *Scr. Mater.*, 2008, **59**(9), 1018–1021.

34 X. Quelennec, A. Menand, J. M. Le Breton, R. Pippan and X. Sauvage, Homogeneous Cu-Fe Supersaturated Solid Solutions Prepared by Severe Plastic Deformation, *Philos. Mag.*, 2010, **90**(9), 1179–1195.

35 C. Zhang, C. Chen, L. Huang, T. Lu, P. Li, W. Wang, F. Yang, A. A. Volinsky and Z. Guo, Microstructure and Properties of Cu-Fe Alloys Fabricated via Powder Metallurgy and Rolling, *Powder Metall*, 2021, **64**(4), 308–320.

36 B. Majumdar, M. M. Raja, A. Narayanasamy and K. Chattopadhyay, Structural and Magnetic Investigations on the Metastable Phases of the Mechanically Alloyed Fe-Cu System, *J. Alloys Compd.*, 1997, **248**(1–2), 192–200.

37 X. Sauvage, F. Wetscher and P. Pareige, Mechanical Alloying of Cu and Fe Induced by Severe Plastic Deformation of a Cu-Fe Composite, *Acta Mater.*, 2005, **53**(7), 2127–2135.

38 A. Puthucode, A. Devaraj, S. Nag, S. Bose, P. Ayyub, M. J. Kaufman and R. Banerjee, De-Vitrification of Nanoscale Phase-Separated Amorphous Thin Films in the Immiscible Copper-Niobium System, *Philos. Mag.*, 2014, **94**(15), 1622–1641.

39 R. Banerjee, A. Puthucode, S. Bose and P. Ayyub, Nanoscale Phase Separation in Amorphous Immiscible Copper-Niobium Alloy Thin Films, *Appl. Phys. Lett.*, 2007, **90**(2), 021904.